Published in final edited form as:

J Drug Deliv Sci Technol. 2023 February ; 80: . doi:10.1016/j.jddst.2022.104093.

Chitosan-graphene quantum dot based active film as smart wound dressing

Elisabete Regina Fernandes Ramos Ribeiro[a], **Luana Barbosa Correa**[a], **Eduardo Ricci-Junior**[b], **Pedro Filho Noronha Souza**[c,d], **Clenilton Costa dos Santos**[e], **Alan Silva de Menezes**[e], **Elaine Cruz Rosas**[f,g], **Prapanna Bhattarai**[h], **Mohamed F. Attia**[i], **Lin Zhu**[h], **Luciana Magalhães Rebelo Alencar**[e], **Ralph Santos-Oliveira**[a,j,*]

[a]Brazilian Nuclear Energy Commission, Nuclear Engineering Institute, Laboratory of Nanoradiopharmaceuticals and Synthesis of Novel Radiopharmaceuticals, Rio de Janeiro, 21941906, Brazil

[b]Federal University of Rio de Janeiro, School of Pharmacy, Galenic Development Laboratory (LADEG), Rio de Janeiro, 21941-170, Brazil

[c]Biochemistry and Molecular Biology Department, Federal University of Ceará, CE, Brazil, Laboratory of Plant Defense Proteins, Ceará, 60451, Brazil

[d]Drug Research and Development Center, Department of Physiology and Pharmacology, Federal, University of Ceará, 60451, Brazil

[e]Federal University of Maranhão, Department of Physics, Laboratory of Biophysics and Nanosystems, Campus Bacanga, São Luís, Maranháo, 65080-805, Brazil

[f]National Institute for Science and Technology on Innovation on Diseases of Neglected Populations (INCT/IDPN), Oswaldo Cruz Foundation, Rio de Janeiro, 21041361, Brazil

[g]Laboratory of Applied Pharmacology, Farmanguinhos, Oswaldo Cruz Foundation, Rio de Janeiro, 21041361, Brazil

[h]Department of Pharmaceutical Sciences, Irma Lerma Rangel College of Pharmacy, Texas A&M University, College Station, TX, 77843, USA

[i]Center for Nanotechnology in Drug Delivery and Division of Pharmaco-engineering and Molecular Pharmaceutics, Eshelman School of Pharmacy, University of North Carolina at Chapel Hill, Chapel Hill, NC, 27599, USA

[*]Corresponding author. Brazilian Nuclear Energy Commission-Nuclear Engineering Institute Rio de Janeiro/RJ, Brazil Rua Hélio de Almeida, 75, Ilha do Fundão, Rio de Janeiro, Brazil. roliveira@ien.gov.br, presidenciaradiofarmacia@gmail.com (R. Santos-Oliveira).

Author statement

Elisabete Regina Fernandes Ramos Ribeiro, Luana Barbosa Correa, Prapanna Bhattarai- Methodology, Formal analysis, Validation, Investigation, Writing - Original Draft, Writing - Review & Editing.

Luciana Magalhães Rebelo Alencar, Mohamed F. Attia, Lin Zhu, Eduardo Ricci-Junior, Elaine Cruz Rosas, Pedro Filho Noronha Souza, Clenilton Costa dos Santos, Alan Silva de Menezes- Methodology, Resources, Data curation, Supervision, Validation, Formal analysis, Writing - Original Draft, Writing - Review & Editing.

Ralph Santos-Oliveira-Conceptualization, Methodology, Validation, Formal analysis, Investigation, Resources, Data curation, Writing - Original Draft, Writing - Review & Editing, Visualization, Supervision, Funding acquisition.

Consent for publication

All authors are in accordance with the publication of this material.

Declaration of competing interest

The authors have declared no conflict of interest.

[j]State University of Rio de Janeiro, Laboratory of Radiopharmacy and Nanoradiopharmaceuticals, Rio de Janeiro, 23070200, Brazil

Abstract

Graphene quantum dots (GQDs), are biocompatible materials, with mechanical strength and stability. Chitosan, has antibacterial and anti-inflammatory properties, and biocompatibility. Wound healing is a challenging process especially in chronic diseases and infection. In this study, films consisting of chitosan and graphene quantum dots were developed for application in infected wounds. The chitosan-graphene films were prepared in the acidic solution followed by slow solvent evaporation and drying. The chitosan-graphene films were characterized by the scanning electron microscopy, x-ray diffraction, atomic force microscopy, Raman spectroscopy and thermogravimetric analysis. The films' was evaluated by the wound healing assays, hemolytic potential, and nitrite production, cytokine production and swelling potential. The obtained films were flexible and well-structured, promoting cell migration, greater antibacterial activity, lower hemolytic activity, and maintaining wound moisture. Our data suggested that the use of graphene quantum dot-containing chitosan films would be an efficient and promising way in combating wounds.

Keywords

Chitosan; Graphene quantum dots; Inflammation; Wound dressing; Cicatrization

1. Introduction

Graphene (G) and its derivatives, including graphene quantum dots (GQDs), are carbon-based nanomaterials with mechanical resistance and stability [1], antimicrobial activity (Kumar et al., 2019), and regenerative activity [2,3]. Graphene quantum dots (GQDs) are quasi-zero-dimensional nanomaterials with low cytotoxicity, great biocompatibility, and excellent water solubility [4].

Chitosan is a biocompatible polysaccharide, derived from exoskeleton of crustaceans, formed mainly by the partial deacetylation of chitin. It is positively charged, due to the presence of quaternary ammonium groups. In addition, chitosan contains several functional groups (C3–OH, C6–OH, C2–NH_2), acetyl amino, and glycoside bonds [5]. Although the functional groups are presented in their structure, the main reactions usually occur with C6–OH and C2–NH_2. This is mainly because of the steric hindrance and fixed axis (not rotating easily) of the acetyl amino and C3–OH that inhibit the reactions [6,7]; J. [8]; W [9]. Chitosan has several interesting characteristics, including: i) immune stimulation (Seferian & Martinez, 2001), ii) antibacterial [10] and antifungal activities [11]; iii) anti-inflammatory activity [12]; iv) hemostatic property [13]; v) biocompatibility [1]; and vi) adhesive property [14,15]. The versatility and adaptability make chitosan an excellent biomaterial for the development of new drugs and devices for human health.

Wound healing is a complex process that involves a cascade of distinct events including hemostasis, inflammation, growth, reepithelialization, and remodeling [16,17]. Several

factors may influence negatively the wound healing process, including: i) failure in immune system; ii) malnutrition, iii) mechanical stress, iv) medical conditions such as: diabetes, vascular disease and obesity, and v) microbial infection [18–20].

Chronic and infected wounds including diabetic foot ulcers, venous leg ulcers and nonhealing surgical wounds are the most challenging types [17,20]. The infected wounds, especially with biofilm, are difficult to treat. In this case, the symbiosis of multi-species presented in the biofilm forms an extracellular polymeric substance (EPS), which protects this microbial community against antimicrobial agents [21,22]. Nonetheless, it is well-known that commensal microorganisms interact with the skin cells during wound healing modulating the innate immune response [20,23,24]. On the other hand, pathogenic microorganisms, especially presented in infected chronic wounds, delayed the epithelialization and altered the cellular signaling, for instance, promoting the down-regulation of keratinocyte growth factor 1 expression [20].

The development of a hydrocolloid dressing formed of graphene quantum dots and chitosan is quite desirable due the synergistic effect. According to Mei et al. [25] chitosan has an innate antimicrobial ability and GQDs may undergo photochemical transformation, producing radical oxygen. The combined effect potentialize the therapeutic effect. In this sense, Hosseini et al. [26] developed nanofibers of chitosan/graphene oxide-magnetite, demonstrating that the presence of graphene oxide-magnetite reduced the burst effect and increased the therapeutic effect of the nanofiber. Finally, Chen et al. [27] developed GQDs modified with chitosan, demonstrating excellent encapsulation and great applicability.

In this study, we prepared and characterized chitosan-GQD-based film, and evaluated its performance as a wound dressing.

2. Materials and methods

2.1. Reagents and solvents

The reagents and solvents used in this study were purchased from Sigma-Aldrich (St. Lois, MO, USA) with exception of the GQDs, which were previously prepared by our laboratory.

2.2. Preparation and characterization of graphene quantum dots (GQDs)

The synthesis and characterization of GQDs were previously described by Menezes and co-workers [28]. In this study, the electrochemical green route was used to produce the GQDs. Briefly, the graphite rod and platinum, respectively anode and cathode, were dispersed in the citric acid/sodium citrate buffer (Sigma-Aldrich, USA). The decomposition of graphite by electrolysis was performed using a constant current of 190 mA for 24 h (ICEL PS-1500; Manaus, Brazil). The dispersion was filtered and dried at 60 °C. Then, 50 mL of absolute ethanol was added. The upper phase (purified graphene) was harvested and dried again at 60 °C. The UV absorbance of the GQDs were detected at 395 nm by UV–Vis (Agilent; Santa Clara, California, USA). The GQDs' size, morphology, and surface texture were determined by the atomic force microscopy (AFM) (Bruker, Santa Barbara, California, USA) (scan resolution of 256 × 256 lines and frequency of 0.5 Hz). The GQDs' fluorescence spectra were determined by the spectrophotometer (Ocean Optics

HR2000, Dunedin, Florida, USA). The composition has been evaluated by powder X-ray diffraction using CuKα radiation source (Bruker AXS D8, Karlsruhe, Germany) and Raman spectroscopy (Horiba-Jobin-Yvon triple model T64000, Palaiseau, Ile de France, France).

2.3. Preparation of chitosan – GQD films

For the preparation of the chitosan films, the chitosan of the medium molecular weight (viscosity 200.000 Cps) was used. A 2% (m/v) chitosan solution was prepared using 2% (v/v) glacial acetic acid under magnetic stirring at 25 °C for 24–36 h for the complete dissolution. For the preparation of the chitosan-GQD films, 5% (w/w%) GQDs was added to the chitosan solution. Then, the solution was poured in Petri dishes (13 cm in diameter) and placed in an oven at 40 ± 0.1 °C for 48 h to promote solvent evaporation. After drying, 200 mL of NaOH solution (1.0 M) was added over the film and maintained for a period of 2 min. Finally, the films were washed with approximately 400 mL of distilled water to completely remove NaOH and dried for 24–48 h at 40 ± 0.1 °C.

2.4. Characterization of chitosan – GQD films

2.4.1. Scanning electron microscopy (SEM)—Scanning Electron Microscopy (SEM) analysis was performed on Hitachi S-4700 Field Emission Microscope. Samples were prepared by sticking the films on a double-stick carbon tape on an aluminum SEM sample holder. The samples were coated with a layer of 7.5 nm Gold–Palladium (AuPd) alloy conductive coating. Operating conditions of Normal mode, 10 kV accelerating voltage, 10microA beam current, and a working distance of close to 12 mm was maintained throughout.

2.4.2. Powder X-ray diffraction (PXRD)—In order to evaluate the characteristics of Chitosan-GQD film, the PXRD measurements were performed using a Bruker AXS D8 Advance diffractometer, equipped with the LynxEye linear detector and with a CuKα radiation source, operating at 40 mA/40 kV. PXRD measurements were carried on the 2θ = 08–90° range with 0.02 step size and a counting time of 0.2s/step.

2.4.3. Atomic Force Microscopy—Chitosan-GQD films were analyzed on an atomic force microscope (model MM8, Bruker). For the analysis was used a probe with a nominal spring constant of 0.4 N/m and a tip radius of 2 nm in quantitative nanomechanics mode the resolution acquired was 256 × 256 samples per line with a scan frequency of 0.5 Hz, and acquisition of force curves at 1 kHz. (Topographic images, young modulus, and adhesion maps were obtained in 10 different film regions.

2.4.4. Raman Spectroscopy—The Raman spectra were obtained using a Triple Raman spectrometer (model T64000, Horiba), operating in the single-model with the slits adjusted to give a resolution lower than 2 cm^{-1}. The instrument was equipped with a liquid-N2-cooled charge-coupled device (CCD) detector. For excitation, a green 532.0 nm line from a solid-state laser (LAS-532–100-HREV) operating at 14 mW was employed. The light was focused on the sample using an Olympus microscopy with a long-work distance (50x, 18 mm) objective lens. The spectra were acquired at different points on the surface of the samples after 3 acquisitions of 30 s each at each range of the grade spectral dispersion.

2.4.5. Thermogravimetric analysis—In the thermogravimetric tests, a thermobalance model TGA-60 (Shimadzu®) was used. The TG/DTG curves were obtained in the temperature range from 30 °C to 600 °C at a heating rate of 10 °C min^{-1}, under a dynamic nitrogen atmosphere (100 mL·min-1). To carry out the tests, a sample mass of 5.00 ± 0.5 mg was used in support of platinum samples. Before the tests, blank curves were obtained to evaluate the baseline of the system. Equipment calibration was performed at a heating rate of 10 °C min^{-1}, with the calcium oxalate standard.

2.5. In vitro assays

2.5.1. Wound-healing assay—The NIH/3T3 fibroblast cells (1.2×10^5) were cultured in 35 mm petri dishes and incubated for 24 h before the experiment. Briefly, a scratch was made on the Petri dish with a 200 μL pipette tip. The cells were washed and the detached cells were removed by the medium. Then, the cells were treated with the chitosan films or chitosan-GQDs film for 8 h. Images were taken using a Nikon Eclipse Ti microscope at 4× magnification and analyzed by the NIS Elements BR software. Wound closure (%) was calculated using the equation:

$$\text{Wound closure } (\%) = \frac{([\text{ scratch width at } 0h] - [\text{ scratch width at } 8h])}{[\text{ scratch width at } 0h]} x100\%$$

2.5.2. Hemolytic assay—The hemolytic activity of the films was tested against all types (A, B, and O) of human red blood cells (HRBC), according to Oliveira et al. (J. T. A [29]. In this direction, three types of HRBCs were chosen to understand the hemolytic effect of the films on different blood types. The HRBCs from A, B and O were provided by the Ceará Hematology and Hemotherapy Center (Brazil).

The blood was collected in the presence of heparin (5 IU/mL) from anonymous healthy donors. The HRB cells were collected by centrifugation at 300*g* for 5 min at 4 °C (Eppendorf Centrifuge 5418/5418R), and dispersed in the 0.15 M sterile NaCl solution. After washing three times with 0.15 M NaCl, HRBCs were diluted to a working concentration of 2.5% by 0.15 M NaCl. Then, an aliquot of 100 μL was incubated with the film (Chitosan-GQDs film) at 5 mg/mL or its vehicle 5% DMSO, individually, and then incubated for 30 min at 37 °C, followed by centrifugation (300 g for 5 min at 4 °C). Afterwards, the supernatants were meticulously collected and transferred to 96-well microtiter plates. Hemolysis (%) was calculated by measuring the presence of hemoglobin in the supernatant at 414 nm on an automated absorbance microplate reader. Negative (0%) and positive (100%) hemolysis were determined by treating HRBCs with 5% DMSO and 0.1% (v/v) Triton X-100, respectively. The hemolysis was calculated as described by Ref. [29].

2.5.3. Bone marrow-derived macrophages—Bone marrow-derived macrophages (BMDMs) were obtained from femurs and tibias of 6-to-8-week-old C57BL/6 mice rinsed with RPMI 1640 (Sigma).

2.5.4. Cells culture—The cells from bone marrow progenitor were seeded in 20 mL RPMI 1640 containing 20% inactivated FBS, 20% of L929 as cell culture supernatant

(v/v) expressing mouse macrophage colony-stimulating factor (M-CSF) and 100 U/mL of penicillin-streptomycin in 140 × 15 mm polystyrene tissue culture dishes at 37 °C in a 5% CO_2 atmosphere. After three days of stimulation, 10 mL of the freshly prepared medium was added. At day seven, the BMDMs were collected for the experiments. The BMDMs were stimulated with lipopolysaccharide (LPS, 100 ng/mL, Sigma-Aldrich) and interferon-(IFN)-γ (20 ng/mL, R&D Systems) or with IL-4 (20 ng/mL, R&D Systems) and IL-13 (20 ng/mL, R&D Systems) to induce polarization towards M1 or M2 phenotypes, respectively. The unstimulated cells acted as a negative control (M0).

2.5.5. Nitrite production—After differentiation, the cells were seeded at a density of 5×10^5 cells/well in 24-well plates and allowed to adhere for 24 h in a controlled atmosphere. Then, the films (Chitosan film and Chitosan – GQD film) were added to the wells together with the stimuli necessary for the polarization of macrophages (LPS and INF-γ for M1 polarization or IL-4 and IL-13 for M2 polarization or RPMI medium for M0). The amount of nitrite, a metabolite of nitric oxide, was assessed in the supernatant from the macrophages using the Griess method. The absorbance was measured at 540 nm in a plate reader (SpectraMax M5, Molecular Devices, Sunnyvale, CA).

2.5.6. Cytokine levels—The level of TNF-α present in the supernatants from BMDM cell culture was quantify by enzyme-linked immunosorbent assay (ELISA) using antibodies obtained from R&D Systems in according to manufacturer's instructions. The optical density of the individual sample was measured at 450 nm (SpectraMax M5, Molecular Devices, Sunnyvale, CA).

2.5.7. Swelling assay—The water absorption test was performed based on the evaluation of the swelling ratio (RI), where there is an increase in volume due to water absorption. Dried films (chitosan film and chitosan-GQDs film) were weighed and immersed in sterile water (20 mL). After 1 h the films were removed from water, the excess of water removed by filter paper and the final mass was determined on an analytical balance (Shimadzu model ATX224).

2.5.8. Statistical analyses—In all experiments, values are expressed as means ± SEM. Differences between groups were tested for significance by one-way ANOVA followed by Tukey multiple comparison tests using GraphPad Prism 5 software. A p value of ≤0.05 was considered significant.

3. Results

3.1. Formulation of chitosan-graphene quantum dots films

After preparation, a flexible, uniform and well-structured chitosan film with GQDs was obtained (Fig. 1), with a thickness of 166.4 ± 5.2 nm and roughness of 19.7 ± 2.3 nm.

3.2. Scanning electron microscopy (SEM)

The SEM analysis is displayed in Fig. 2. The data indicated that the presence of GQDs influenced the structural organization of the chitosan film.

3.3. Powder X-ray diffraction

The X-ray diffraction analysis demonstrated that the main components of the formulation were detected as demonstrated in Fig. 3.

3.4. Atomic Force Microscopy

The AFM results presented in Fig. 4 show a 10 μm scan over the chitosan-GQD film. The mean square roughness of the film was 19.7 ± 5.2 nm. The striated regions shown in Fig. 4A are associated with the film's stretching process. Young's modulus (YM) values are in the order of MPa (Fig. 4C). The lighter regions with higher YM values shown in Fig. 4C probably correspond to areas with higher concentrations of GQDs. The adhesion map shown in Fig. 4D also reveals the heterogeneous behavior of the film surface, with two distinct phases in the film, 1 and 2, respectively, related to the chitosan matrix and the insertion of quantum dots into it.

3.5. Raman Spectroscopy

The Raman spectra demonstrated the presence of graphene in the chitosan film produced. (Fig. 5). Despite of the high concentration of chitosan in the film, the Raman was not able to detect the characteristic bands of chitosan. This is explained by the fact that during the film preparation, chitosan is probably converted into an amorphous composite, which modifies the original spectra.

3.6. Thermogravimetric analysis (TGA)

The TGA analysis (Fig. 6A) showed a loss of water starting in the range of 60–100 °C with a massive loss of water in the range of 150–200 °C and the formation of oxide (chitosan oxide) in the range of 250–300 °C. In the film containing GQDs a pronounced loss of water was observed in the range of 100–250 °C and a massive formation of oxide (graphene oxide plus chitosan oxide) started at 300 °C.

3.7. In vitro assays

3.7.1. Wound healing assay—The results of the wound healing assay are shown in Fig. 7. After 8 h of treatments, both the chitosan film and chitosan-GQD film facilitated the wound healing process. The effects were the dose-dependent. Particularly, at high dose, the chitosan-GQD film treated cells demonstrated more than 20% higher wound closure than the untreated cells.

3.7.2. Hemolytic assay—The hemolytic assay demonstrated (Fig. 8) that the film didn't significantly cause the hemolysis among all types of blood.

3.7.3. M1 and M2 macrophage stimuli response—We tested the effect of the chitosan-GQD film on macrophage polarization. When we evaluated the effect of films on nitric oxide production, it was observed that Chitosan-GQD film did not influence in both M1 and M2 macrophages, demonstrating a neutral profile (Fig. 9A) i.e., the results obtained in this assay demonstrated that the incubation of cells with both Chitosan and Chitosan–GQD films did not lead to a reduction in the production of nitric oxide (NO) in

macrophages polarized for the M1 profile. But biofilms also didn't induce NO production in macrophages polarized for the M2 or M0 profile, what showed that they do not have an anti- or pro-inflammatory effect.

However, when we evaluated the TNF-α cytokine production, a significant increase in the TNF-α level was observed in the M1 macrophages (Fig. 9B).

3.7.4. Swelling assay—The adsorption of water was evaluated (Fig. 10) and the values are expressed in Table 1.

The results demonstrated that the chitosan-GQD film was more likely to absorb water than the chitosan film.

4. Discussion

The use of polymer films for wound dressing applications are based not only on their ability to form the physical barrier and remove the exudate, but also to perfectly fill the irregularly shaped wounds avoiding deep bleeding. Indeed, films are able to provide a moisture environment that promotes the wound healing process as they prevent the entry of bacteria [30]. The Chitosan-GQD film showed a thickness of 166.4 nm and roughness of 19.7 nm by the AFM analysis. The roughness is probably due to the presence of graphene quantum dots in the film. The film thickness is quite important because the thinner the film is, the better the oxygenation would be. According to Kundu et al. [31], the photocatalytic activity increased with the increase in the film thickness from 50 to 500 nm.

The results of the DRX and Raman analysis corroborated the presence of chitosan and graphene quantum dots in the formulation. The characteristic bands of "2D" graphite were observed in the Raman spectra. This may be explained by the fact that during the film preparation, the graphene quantum dots aggregated with the changed size and shape, giving the graphite signal (Rocher & Ambacher, 2019). The SEM analysis demonstrated the influence of GQDs on the nanostructure of the film. Martín et al. (Although Martín et al., 2019) stated that GQDs were unable to form the bonds and integrate the polymeric network in hydrogels. However, in our study, the SEM images revealed that GQDs were able to integrate into the Chitosan film, forming the homogeneous films. Although the GQDs modified the film structure and formed the hybrid film without phase separation, their influence on the film mechanical properties and stability was not significant. The TGA analysis demonstrated the presence of water in the film and the formation of oxide at high temperatures [32].

Graphene quantum dots have shown the antibacterial activity, probably due to their ability to disrupt the bacterial cell envelop [33]. Also, microbial respiration is based on electron transfer from electron donors to electron acceptors, mediated by a complex cascade of energetic substances [34–38]. The donors and acceptors of electrons are typically soluble substances; however, some microorganisms can use solid electron donors and/or solid electron acceptors, such as minerals and metals, in respiration [39]. The GQDs are recognized as an excellent electron donor [40–42] and allow the microbial respiration,

especially the beneficial bacteria, such as *S. epidermidis*, which plays a critical role in skin immunity [43].

Another important aspect is the production of oxygen. According to Ochoa et al. [44], one of the most critical points in the treatment of wounds is the right oxygenation of the wound bed. In this regard, the GQDs have shown the ability to generate the local oxygen [45], which may serve as a topical oxygen therapy (TOT) to promote the wound healing.

The hemolytic data showed that Chitosa-GQD film had no significant hemolytic activity. This was corroborated by the work of Lima et al. [46] that demonstrated that the chitosan-nanoparticles had higher hemagglutination index and lower hemolytic activity in human erythrocytes than chitosan (conventional). Guo et al. [47] also confirmed that chitosan has no effect on hemolysis in their study. Regarding the effect of graphene quantum dots on hemolysis the literature is quite divergent. For instance, Qu et al. [48] demonstrated that graphene quantum dots had hemolytic effect on red blood cells. Controversially, Kim et al. [49] stated that graphene quantum dots at a dose of <500 μg/mL didin't cause any hemolytic effects. In our study, we believed that the immobilization of GQDs in the chitosan film, might inhibit the GQDs' hemolytic effects on red blood cells.

The M1 and M2 response stimuli showed a neutral profile, i.e., did not promote a pro-inflammatory or an anti-inflammatory response. However, the TNF-α cytokine production showed a significant increase when M1 macrophages were in contact with the chitosan-GQD film. Here, the direct contact of biomaterials (chitosan and GQDs) with the cells might exert the stress on the cells, leading to the production of some inflammatory mediators. Oliveira et al. (M. I [50]. showed the chitosan film-induced macrophage and dendritic cell activation and found that chitosan was capable of modulating macrophage polarization towards an M2 phenotype.

The swelling assay showed that Chitosan-GQDs film was able to absorb more water than the pure chitosan film, probably due to the GQDs' swelling behavior [51]. This data showed that the film was able to keep moisture and humidity in the wounds. According to Jones et al. (Jones et al., 2006), a balanced humidity is crucial for the healing process, especially considering that occlusive dressings (as the films developed) increase cell proliferation and activity by retaining an optimum level of wound exudate. The presence of graphene quantum dots in the film increased the absorption of water, which means that the wound will keep the necessary moisture as the exudate, improving the healing process.

The wound healing assay demonstrated that both the chitosan film and chitosan-GQD film could facilitate the cell migration and wound healing process in a dose-dependent manner. This data is consistent with the previous report [52] that the hydrogel containing quaternized chitosan-g-polyaniline (QCSP) and benzaldehyde group functionalized poly (ethylene glycol)-co-poly (glycerol sebacate) (PEGS-FA) showed the excellent antibacterial activity, in vivo blood clotting, and promotion of full skin wound healing. Also, Zmejkoski et al. [53] demonstrated that bacterial cellulose (BC) impregnated with graphene quantum dots (GQDs) could benefit the wound healing treatment.

5. Conclusion

Dressings with biocompatible films are promising for wound care. Due to the abilities to maintain a favorable environment, form a physical barrier, as well as prevent the entry of bacteria, collaborating for a balanced environment.

The chitosan graphene quantum dot film produced in the present study has shown the very relevant properties, supporting its later implementation in wound care. The film showed promising results in all tests carried out and congruence with the parameters correlated to positive wound care. The developed chitosan-graphene quantum dot film might be a promising innovative dressing in the fight against wounds.

Funding

This study was funded by Carlos Chagas Filho Foundation for Research Support of Rio de Janeiro State (FAPERJ) (Cientista do Nosso Estado:E–26/200.815/2021; Rede NanoSaude: E–26/010.000981/2019, Pesquisa na UEZO: E–26/010.002362/2019; Temáticos: E–26/211.269/2021, Infraestrutura e Pesquisa na UEZO e UERJ: E–26//211.207/2021, Bolsa de Pós Doutorado Senior (PDS):E 26/202.320/2021) CNPq (Bolsa de Produtividade 1B: 301069/2018–2) to Ralph Santos-Oliveira. Also, the work was partially supported by the National Cancer Institute of the National Institutes of Health (R15CA213103) to Dr. Lin Zhu.

Availability of data and materials

All data will be available under request.

References

[1]. Meng Q, Sun Y, Cong H, Hu H, Xu FJ, An overview of chitosan and its application in infectious diseases, Drug Delivery and Translational Research 11 (4) (2021) 1340, 10.1007/S13346-021-00913-W. [PubMed: 33496926]

[2]. Bellet P, Gasparotto M, Pressi S, Fortunato A, Scapin G, Mba M, Menna E, Filippini F, Graphene-based scaffolds for regenerative medicine, Nanomaterials 11 (2) (2021) 1–41, 10.3390/nano11020404.

[3]. Kenry, Lee WC, Loh KP, Lim CT, When stem cells meet graphene: opportunities and challenges in regenerative medicine, Biomaterials 155 (2018) 236–250, 10.1016/j.biomaterials.2017.10.004. [PubMed: 29195230]

[4]. Kishida H, Mikkelsen MH, Ultrafast lifetime and bright emission from graphene quantum dots using plasmonic nanogap cavities, Nano Lett. 22 (3) (2022) 904–910, 10.1021/ACS.NANOLETT.1C03419/SUPPL_FILE/NL1C03419_SI_001.PDF. [PubMed: 35044773]

[5]. Razmi FA, Ngadi N, Wong S, Inuwa IM, Opotu LA, Kinetics, thermodynamics, isotherm and regeneration analysis of chitosan modified pandan adsorbent, J. Clean. Prod 231 (2019) 98–109, 10.1016/J.JCLEPRO.2019.05.228.

[6]. Braz EMA, Silva SCCC, Sousa Brito CAR, Brito LM, Barreto HM, Carvalho FAA, Santos LS, Lobo AO, Osajima JA, Sousa KS, Silva-Filho EC, Spectroscopic, thermal characterizations and bacteria inhibition of chemically modified chitosan with phthalic anhydride, Mater. Chem. Phys 240 (2020), 122053, 10.1016/J.MATCHEMPHYS.2019.122053.

[7]. Medeiros Borsagli FGL, Carvalho IC, Mansur HS, Amino acid-grafted and Nacylated chitosan thiomers: construction of 3D bio-scaffolds for potential cartilage repair applications, Int. J. Biol. Macromol 114 (2018) 270–282, 10.1016/J.IJBIOMAC.2018.03.133. [PubMed: 29578009]

[8]. Wang J, Wang L, Yu H, Zain-ul-Abdin, Chen Y, Chen Q, Zhou W, Zhang H, Chen X, Recent progress on synthesis, property and application of modified chitosan: an overview, Int. J. Biol. Macromol 88 (2016) 333–344, 10.1016/J.IJBIOMAC.2016.04.002. [PubMed: 27044349]

[9]. Wang W, Meng Q, Li Q, Liu J, Zhou M, Jin Z, Zhao K, Chitosan derivatives and their application in biomedicine, Int. J. Mol. Sci 21 (2) (2020), 10.3390/IJMS21020487.

[10]. Ardean C, Davidescu CM, Nemes NS, Negrea A, Ciopec M, Duteanu N, Negrea P, Duda-seiman D, Musta V, Factors influencing the antibacterial activity of chitosan and chitosan modified by functionalization, Int. J. Mol. Sci 22 (14) (2021), 10.3390/IJMS22147449.

[11]. Wardana AA, Koga A, Tanaka F, Tanaka F, Antifungal features and properties of chitosan/sandalwood oil Pickering emulsion coating stabilized by appropriate cellulose nanofiber dosage for fresh fruit application, Sci. Rep 11 (1) (2021), 10.1038/S41598-021-98074-W.

[12]. Yi P, Xu X, Qiu B, Li H, Impact of chitosan membrane culture on the expression of pro- and anti-inflammatory cytokines in mesenchymal stem cells, Exp. Ther. Med 20 (4) (2020), 10.3892/ETM.2020.9108.

[13]. Narvaez-Flores J, Vilar-Pineda G, Acosta-Torres L, Garcia-Contreras R, Cytotoxic and anti-inflammatory effects of chitosan and hemostatic gelatin in oral cell culture, Acta Odontol. Latinoam. : AOL 34 (2) (2021) 98–103, 10.54589/AOL.34/2/098. [PubMed: 34570856]

[14]. Bharadwaz A, Jayasuriya AC, Recent trends in the application of widely used natural and synthetic polymer nanocomposites in bone tissue regeneration, Materials Science & Engineering. C, Materials for Biological Applications 110 (2020), 10.1016/J.MSEC.2020.110698.

[15]. Burhan AM, Klahan B, Cummins W, Andrés-Guerrero V, Byrne ME, O'reilly NJ, Chauhan A, Fitzhenry L, Hughes H, Posterior segment ophthalmic drug delivery: role of muco-adhesion with a special focus on chitosan, Pharmaceutics 13 (10) (2021), 10.3390/PHARMACEUTICS13101685.

[16]. Bowler PG, Parsons D, Combatting wound biofilm and recalcitrance with a novel anti-biofilm Hydrofiber® wound dressing, Wound Medicine 14 (2016) 6–11, 10.1016/J.WNDM.2016.05.005.

[17]. Rodrigues M, Kosaric N, Bonham CA, Gurtner GC, Wound healing: a cellular perspective, Physiol. Rev 99 (1) (2019) 665, 10.1152/PHYSREV.00067.2017. [PubMed: 30475656]

[18]. Eming SA, Martin P, Tomic-Canic M, Wound repair and regeneration: mechanisms, signaling, and translation, Sci. Transl. Med 6 (265) (2014), 10.1126/SCITRANSLMED.3009337.

[19]. Fayne RA, Borda LJ, Egger AN, Tomic-Canic M, The potential impact of social genomics on wound healing, Adv. Wound Care 9 (6) (2020) 325, 10.1089/WOUND.2019.1095.

[20]. Tomic-Canic M, Burgess JL, O'Neill KE, Strbo N, Pastar I, Skin microbiota and its interplay with wound healing, Am. J. Clin. Dermatol 21 (Suppl 1) (2020) 36, 10.1007/S40257-020-00536-W. [PubMed: 32914215]

[21]. Greer HM, Overton K, Ferguson MA, Spain EM, Darling LEO, Núñez ME, Volle CB, Extracellular polymeric substance protects some cells in an Escherichia coli biofilm from the biomechanical consequences of treatment with magainin 2, Microorganisms 9 (5) (2021), 10.3390/MICROORGANISMS9050976.

[22]. Hahn MM, González JF, Gunn JS, Salmonella biofilms tolerate hydrogen peroxide by a combination of extracellular polymeric substance barrier function and catalase enzymes, Front. Cell. Infect. Microbiol 11 (2021), 10.3389/FCIMB.2021.683081.

[23]. Harrison OJ, Linehan JL, Shih HY, Bouladoux N, Han SJ, Smelkinson M, Sen SK, Byrd AL, Enamorado M, Yao C, Tamoutounour S, Van Laethem F, Hurabielle C, Collins N, Paun A, Salcedo R, O'Shea JJ, Belkaid Y, Commensalspecific T Cell Plasticity Promotes Rapid Tissue Adaptation to Injury, Science, New York, N.Y.), 2019, p. 363, 10.1126/SCIENCE.AAT6280, 6422.

[24]. Lai Y, Di Nardo A, Nakatsuji T, Leichtle A, Yang Y, Cogen AL, Wu ZR, Hooper LV, Schmidt RR, Von Aulock S, Radek KA, Huang CM, Ryan AF, Gallo RL, Commensal bacteria regulate TLR3-dependent inflammation following skin injury, Nat. Med 15 (12) (2009) 1377, 10.1038/NM.2062. [PubMed: 19966777]

[25]. Mei L, Gao X, Shi Y, Cheng C, Shi Z, Jiao M, Cao F, Xu Z, Li X, Zhang J, Augmented graphene quantum dot-light irradiation therapy for bacteria-infected wounds, Sep. 9, ACS Appl. Mater. Interfaces 12 (36) (2020) 40153–40162, 10.1021/acsami.0c13237. Epub 2020 Aug 25. [PubMed: 32805864]

[26]. Hosseini SM, Abdouss M, Mazinani S, Soltanabadi A, Kalaee M, Modified nanofiber containing chitosan and graphene oxide-magnetite nanoparticles as effective materials for smart wound

dressing, Compos. B Eng 231 (2022), 109557, 10.1016/j.compositesb.2021.109557. ISSN 1359–8368.

[27]. Chen L, Hong W, Duan S, Li Y, Wang J, Zhu J, Graphene quantum dots mediated magnetic chitosan drug delivery nanosystems for targeting synergistic photothermal-chemotherapy of hepatocellular carcinoma, Cancer Biol. Ther 23 (1) (2022) 281–293, 10.1080/15384047.2022.2054249, 2022 Dec 31. [PubMed: 35323086]

[28]. de Menezes FD, dos Reis SRR, Pinto SR, Portilho FL, do Vale Chaves e Mello F, Helal-Neto E, da Silva de Barros AO, Alencar LMR, de Menezes AS, dos Santos CC, Saraiva-Souza A, Perini JA, Machado DE, Felzenswalb I, Araujo-Lima CF, Sukhanova A, Nabiev I, Santos-Oliveira R, Graphene quantum dots unraveling: green synthesis, characterization, radiolabeling with 99mTc, in vivo behavior and mutagenicity, Mater. Sci. Eng. C 102 (2019) 405–414, 10.1016/J.MSEC.2019.04.058.

[29]. Oliveira JTA, Souza PFN, Vasconcelos IM, Dias LP, Martins TF, van Tilburg MF, Guedes MIF, Sousa DOB, Mo-CBP3-PepI, Mo-CBP3-PepII, and Mo-CBP3-PepIII are synthetic antimicrobial peptides active against human pathogens by stimulating ROS generation and increasing plasma membrane permeability, Biochimie 157 (2019) 10–21, 10.1016/J.BIOCHI.2018.10.016. [PubMed: 30389515]

[30]. Pan Z, Ye H, Wu D, Recent advances on polymeric hydrogels as wound dressings, APL Bioengineering 5 (1) (2021), 011504, 10.1063/5.0038364. [PubMed: 33644627]

[31]. Kundu S, Kafizas A, Hyett G, Mills A, Darr JA, Parkin IP, An investigation into the effect of thickness of titanium dioxide and gold–silver nanoparticle titanium dioxide composite thin-films on photocatalytic activity and photo-induced oxygen production in a sacrificial system, J. Mater. Chem 21 (19) (2011) 6854–6863, 10.1039/C0JM03492D.

[32]. Yan R, Wu H, Zheng Q, Wang J, Huang J, Ding K, Guo Q, Wang J, Graphene quantum dots cut from graphene flakes: high electrocatalytic activity for oxygen reduction and low cytotoxicity, RSC Adv. 4 (44) (2014) 23097–23106, 10.1039/C4RA02336F.

[33]. Hui L, Huang J, Chen G, Zhu Y, Yang L, Antibacterial property of graphene quantum dots (both source material and bacterial shape matter), ACS Appl. Mater. Interfaces 8 (1) (2016) 20–25, 10.1021/ACSAMI.5B10132/SUPPL_FILE/AM5B10132_SI_001.PDF. [PubMed: 26696468]

[34]. Babauta J, Renslow R, Lewandowski Z, Beyenal H, Electrochemically active biofilms: facts and fiction. A review, Biofouling 28 (8) (2012) 789, 10.1080/08927014.2012.710324. [PubMed: 22856464]

[35]. Bird LJ, Bonnefoy V, Newman DK, Bioenergetic challenges of microbial iron metabolisms, Trends Microbiol. 19 (7) (2011) 330–340, 10.1016/J.TIM.2011.05.001. [PubMed: 21664821]

[36]. Gralnick JA, Newman DK, Extracellular respiration, Mol. Microbiol 65 (1) (2007) 1, 10.1111/J.1365-2958.2007.05778.X. [PubMed: 17581115]

[37]. Kraft B, Strous M, Tegetmeyer HE, Microbial nitrate respiration – genes, enzymes and environmental distribution, J. Biotechnol 155 (1) (2011) 104–117, 10.1016/J.JBIOTEC.2010.12.025. [PubMed: 21219945]

[38]. Stams AJM, De Bok FAM, Plugge CM, Van Eekert MHA, Dolfing J, Schraa G, Exocellular electron transfer in anaerobic microbial communities, Environ. Microbiol 8 (3) (2006) 371–382, 10.1111/J.1462-2920.2006.00989.X. [PubMed: 16478444]

[39]. Nealson KH, Finkel SE, Electron flow and biofilms, MRS Bull. 36 (5) (2011) 380–384, 10.1557/MRS.2011.69, 2011 36:5.

[40]. Huang D, Yin L, Lu X, Lin S, Niu Z, Niu J, Directional electron transfer mechanisms with graphene quantum dots as the electron donor for photodecomposition of perfluorooctane sulfonate, Chem. Eng. J 323 (2017) 406–414, 10.1016/J.CEJ.2017.04.124.

[41]. Long R, Casanova D, Fang WH, Prezhdo OV, Donor-acceptor interaction determines the mechanism of photoinduced electron injection from graphene quantum dots into TiO2: π-stacking supersedes covalent bonding, J. Am. Chem. Soc 139 (7) (2017) 2619–2629, 10.1021/JACS.6B09598/ASSET/IMAGES/LARGE/JA-2016-095982_0004.JPEG. [PubMed: 28125783]

[42]. Privitera A, Righetto M, Mosconi D, Lorandi F, Isse AA, Moretto A, Bozio R, Ferrante C, Franco L, Boosting carbon quantum dots/fullerene electron transfer via surface group engineering, Phys. Chem. Chem. Phys 18 (45) (2016) 31286–31295, 10.1039/C6CP05981C. [PubMed: 27824179]

[43]. Maheswary T, Nurul AA, Fauzi MB, The insights of microbes' roles in wound healing: a comprehensive review, Pharmaceutics 13 (7) (2021) 981, 10.3390/PHARMACEUTICS13070981. [PubMed: 34209654]

[44]. Ochoa M, Rahimi R, Zhou J, Jiang H, Yoon CK, Maddipatla D, Narakathu BB, Jain V, Oscai MM, Morken TJ, Oliveira RH, Campana GL, Cummings OW, Zieger MA, Sood R, Atashbar MZ, Ziaie B, Integrated sensing and delivery of oxygen for next-generation smart wound dressings, Microsystems & Nanoengineering 6 (1) (2020) 1–16, 10.1038/s41378-020-0141-7, 2020 6:1. [PubMed: 34567616]

[45]. Jovanović SP, Syrgiannis Z, Budimir MD, Milivojević DD, Jovanovic DJ, Pavlović VB, Papan JM, Bartenwerfer M, Mojsin MM, Stevanović MJ, Todorović Marković BT, Graphene quantum dots as singlet oxygen producer or radical quencher - the matter of functionalization with urea/thiourea, Mater. Sci. Eng. C 109 (2020), 110539, 10.1016/J.MSEC.2019.110539.

[46]. De Lima JM, Sarmento RR, De Souza JR, Brayner FA, Feitosa APS, Padilha R, Alves LC, Porto IJ, Batista RFBD, De Oliveira JE, De Medeiros ES, Bonan PRF, Castellano LR, Evaluation of hemagglutination activity of chitosan nanoparticles using human erythrocytes, BioMed Res. Int (2015), 10.1155/2015/247965, 2015.

[47]. Guo X, Sun T, Zhong R, Ma L, You C, Tian M, Li H, Wang C, Effects of chitosan oligosaccharides on human blood components, Front. Pharmacol 9 (2018) 1412, 10.3389/FPHAR.2018.01412/PDF. [PubMed: 30559672]

[48]. Qu G, Wang X, Wang Z, Liu S, Jiang G, Cytotoxicity of quantum dots and graphene oxide to erythroid cells and macrophages, Nanoscale Res. Lett 8 (1) (2013) 1–9, 10.1186/1556-276X-8-198/FIGURES/7. [PubMed: 23279756]

[49]. Kim J, Nafiujjaman M, Nurunnabi M, Lee YK, Park HK, Hemorheological characteristics of red blood cells exposed to surface functionalized graphene quantum dots, Food Chem. Toxicol : An International Journal Published for the British Industrial Biological Research Association 97 (2016) 346–353, 10.1016/J.FCT.2016.09.034. [PubMed: 27697543]

[50]. Oliveira MI, Santos SG, Oliveira MJ, Torres AL, Barbosa MA, Chitosan drives anti-inflammatory macrophage polarisation and pro-inflammatory dendritic cell stimulation, Eur. Cell. Mater 24 (2012) 136–153, 10.22203/ECM.V024A10. [PubMed: 22828991]

[51]. Laysandra L, Kurniawan D, Wang CL, Chiang WH, Chiu YC, Synergistic effect in a graphene quantum dot-enabled luminescent skinlike copolymer for long-term pH detection, ACS Appl. Mater. Interfaces 13 (50) (2021) 60413–60424, 10.1021/ACSAMI.1C18077. [PubMed: 34894653]

[52]. Zhao X, Wu H, Guo B, Dong R, Qiu Y, Ma PX, Antibacterial anti-oxidant electroactive injectable hydrogel as self-healing wound dressing with hemostasis and adhesiveness for cutaneous wound healing, Biomaterials 122 (2017) 34–47, 10.1016/J.BIOMATERIALS.2017.01.011. [PubMed: 28107663]

[53]. Zmejkoski DZ, Marković ZM, Mitić DD, Zdravković NM, Kozyrovska NO, Bugárová N, Todorović Marković BM, Antibacterial composite hydrogels of graphene quantum dots and bacterial cellulose accelerate wound healing, J. Biomed. Mater. Res. B Appl. Biomater 110 (8) (2022), 10.1002/JBM.B.35037.

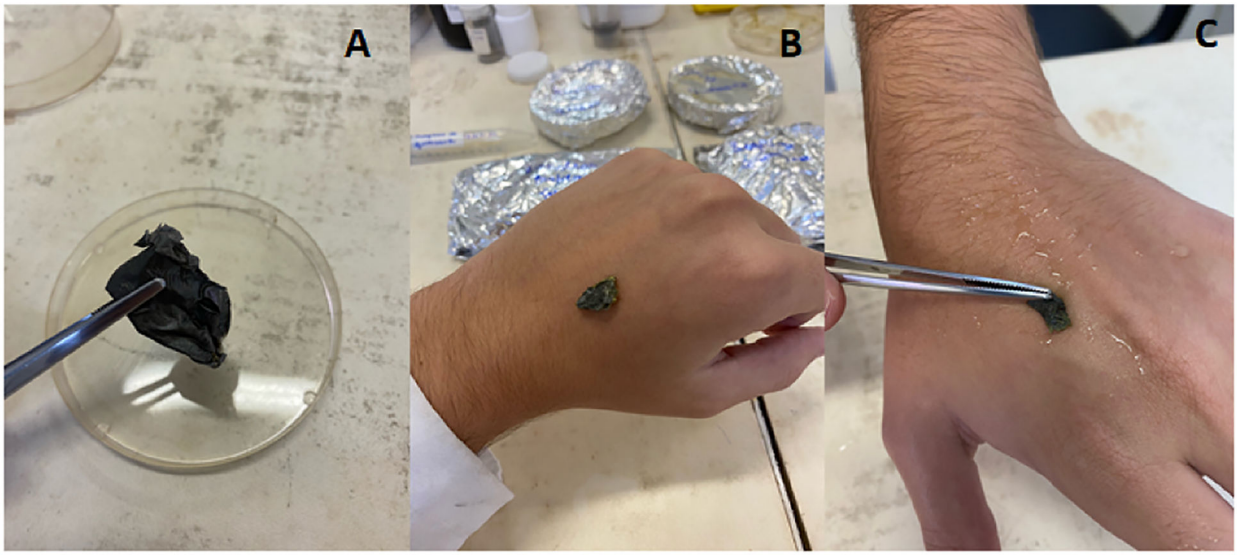

Fig. 1.

A: The dry chitosan-GQD films. B: in the absence of water, no adherence of the films on the skin is observed. C: after humidifying the skin with water, the adherence of the films on the skin is observed.

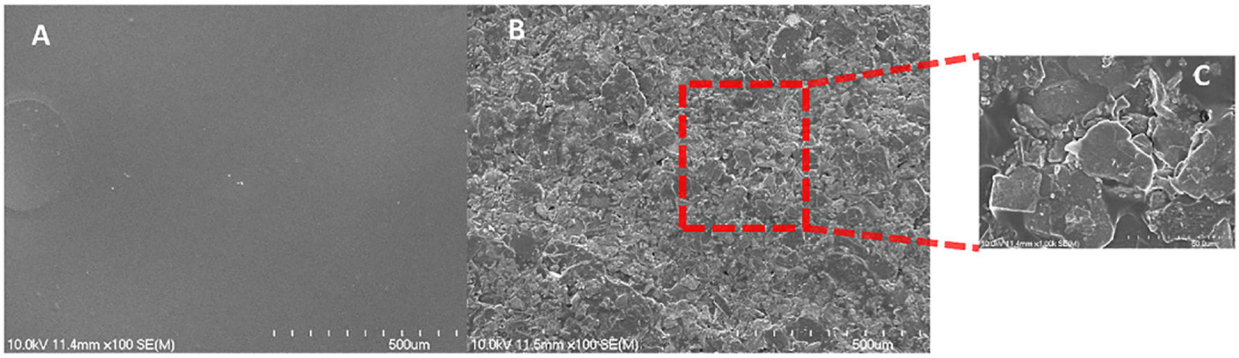

Fig. 2.

Scanning electron microscopy (SEM) of the chitosan-GQD films produced. A, the chitosan film at a 100X amplification; B, the chitosan-GQD film at a 100X amplification; and C, the chitosan-GQD film a 1000X amplification.

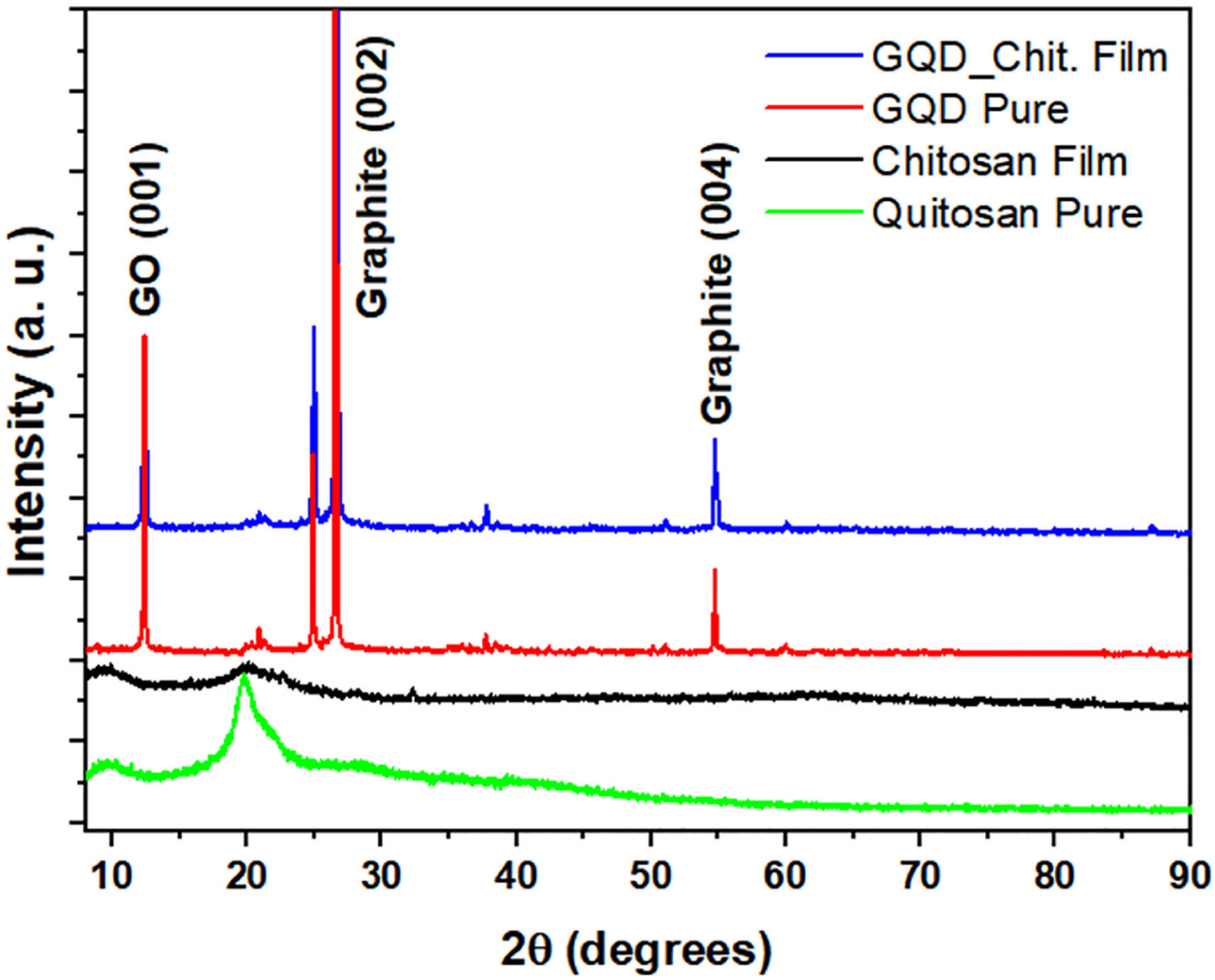

Fig. 3.

Powder X-ray Diffraction: Chitosan film (black); Chitosan (green); graphene (Red); Chitosan-GQD film (blue). (For interpretation of the references to color in this figure legend, the reader is referred to the Web version of this article.)

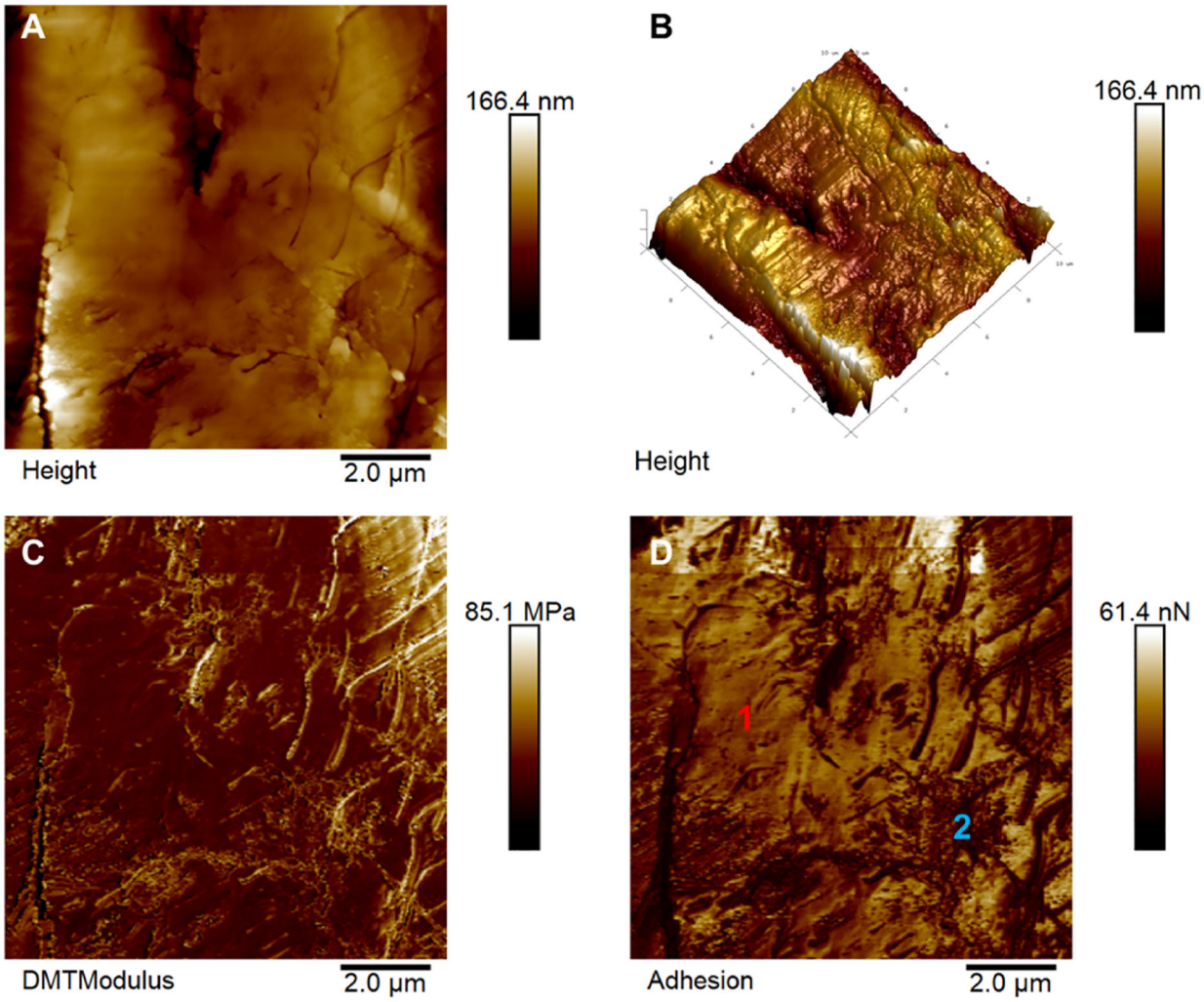

Fig. 4.

Atomic Force Microscopy of maps of chitosan-GQD films. A) Two-dimensional topographical image and B) its respective three-dimensional representation of the film surface. C) Young's modulus map and D) surface adhesion forces map corresponding to the film's region shown in A) Regions 1 and 2 indicate the film's two phases related to the chitosan matrix and the GQDs.

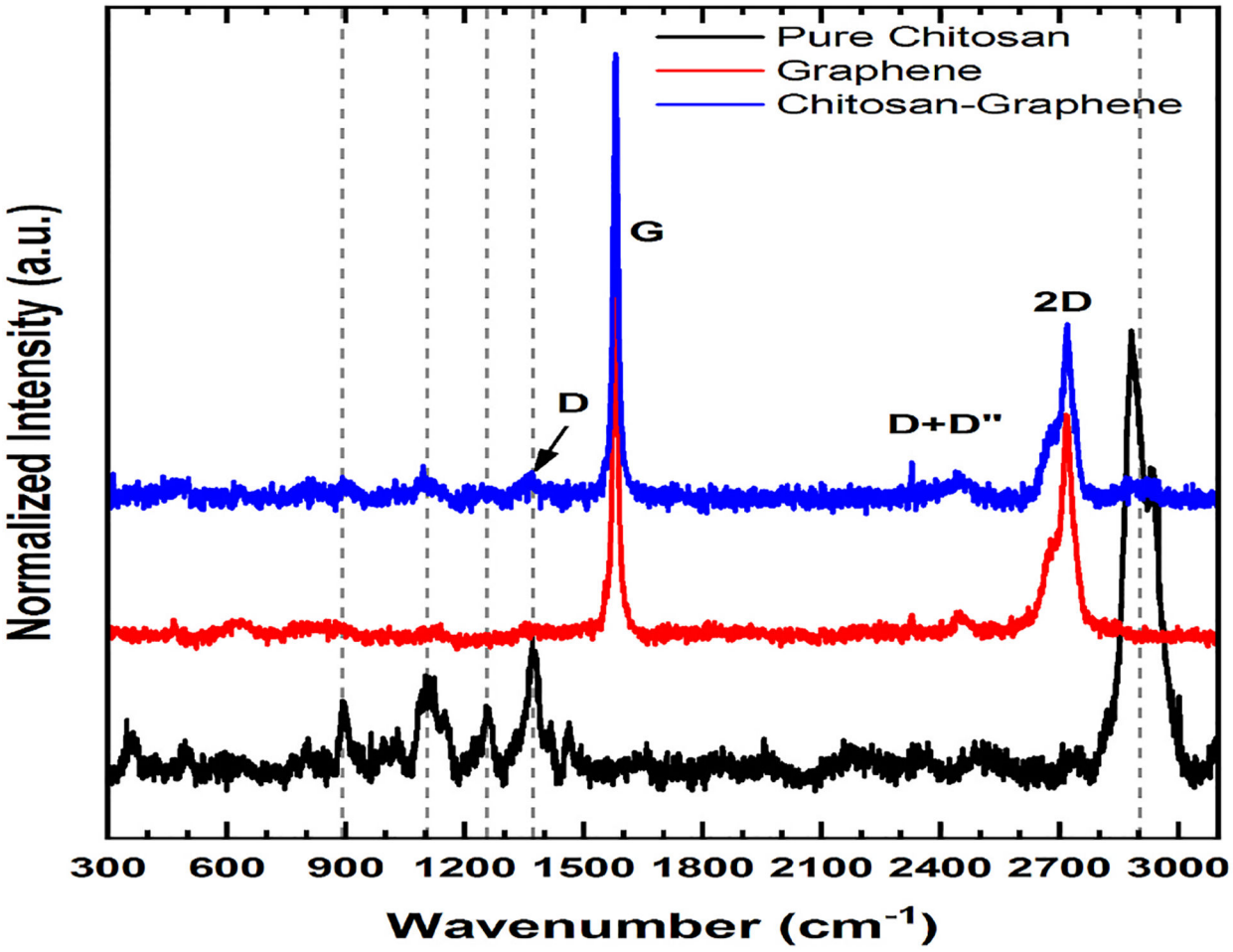

Fig. 5.

Raman Spectroscopy of Pure Chitosan (black), Graphene (red) and Chitosan-GQD film (blue). (For interpretation of the references to color in this figure legend, the reader is referred to the Web version of this article.)

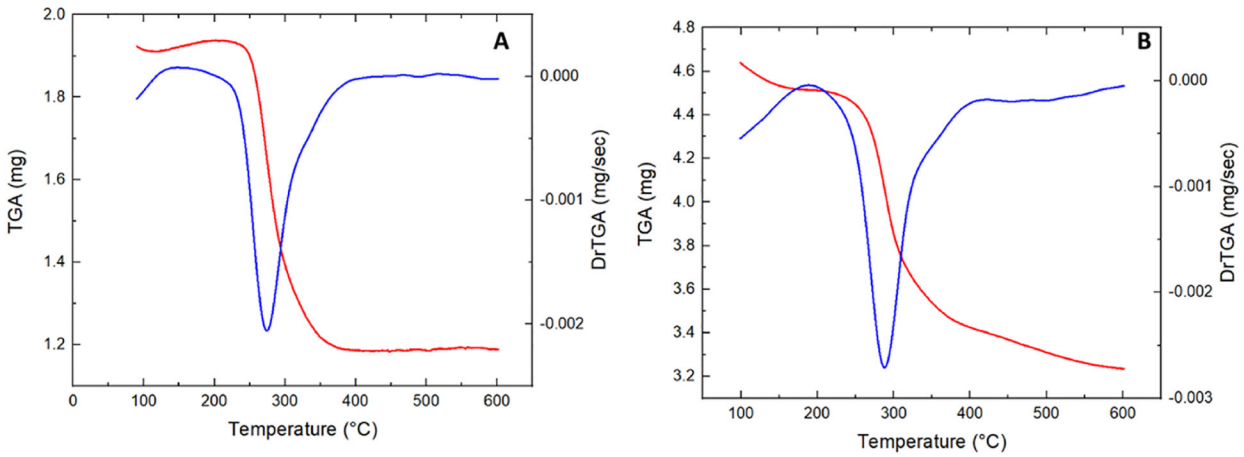

Fig. 6.

TGA analysis of pure Chitosan film (A) and Chitosan-GQD film (B). The loss of water and the formation of oxides were observed, especially at high temperatures (300 °C).

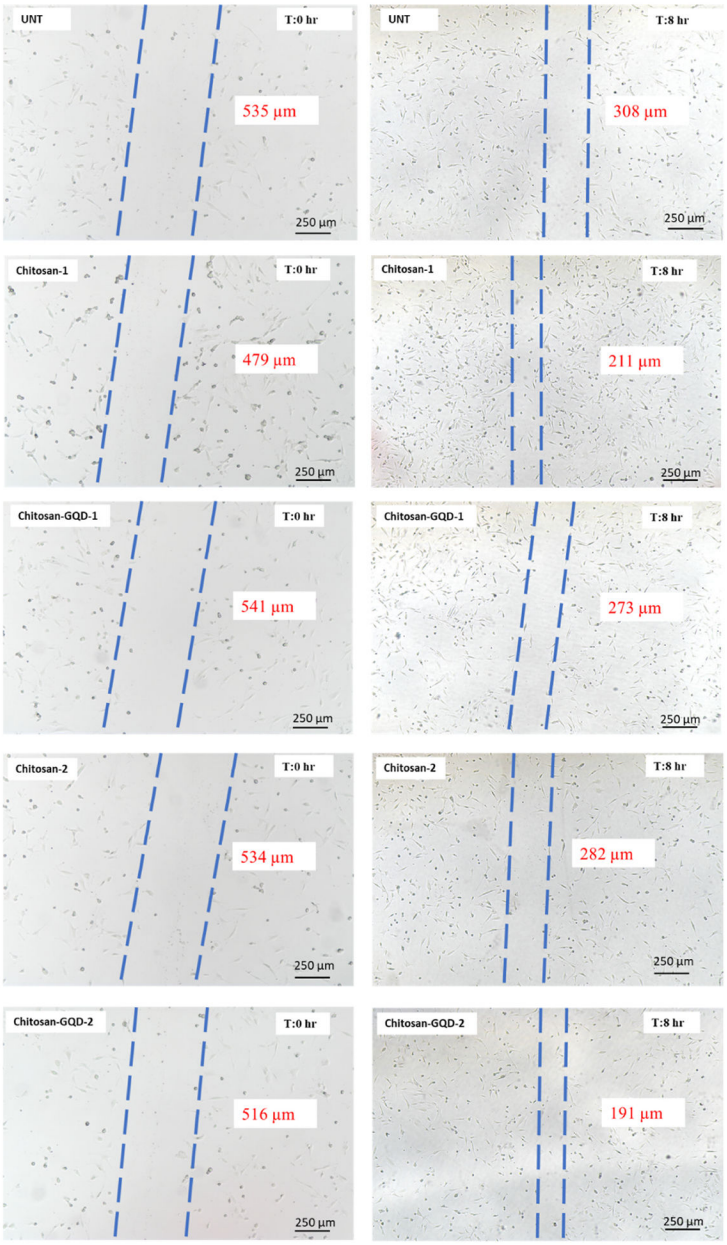

Fig. 7.

Wound healing assay. The films were applied over the NIH/3T3 cells in two strengths: 0.13 mg/mL (chitosan-1 and chitosan-GQD −1) or 0.79 mg/mL (chitosan-2 and chitosan-GQD-2). The width of the scratch (region between the dashed lines) is expressed by the values in red. (For interpretation of the references to color in this figure legend, the reader is referred to the Web version of this article.)

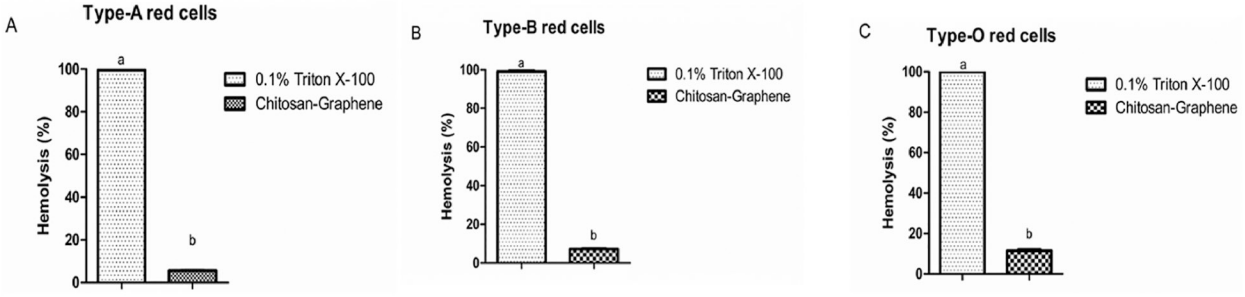

Fig. 8.

Hemolytic assay in human red blood cells. In all cases Chitosan-GQD film is unable to produce hemolysis.

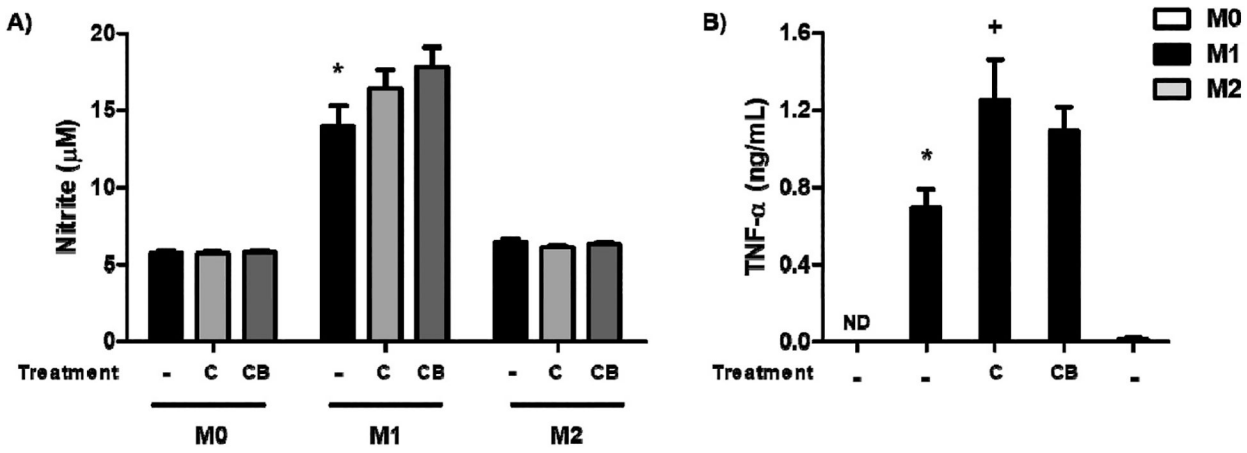

Fig. 9.

Effects of the chitosan-GQD film on macrophages. BMDMs were polarized into M1 or M2, and then the chitosan-GQDs film [C] and chitosan film [CB] were added and incubated for 24 h or 48 h. For the M1 differentiation, BMDMs were stimulated with LPS (100 ng/mL) and IFN-γ (20 ng/mL) for 24 h. For the M2 differentiation, cells were cultured with IL-4 (20 ng/mL) and IL-13 (20 ng/mL) for 48 h; unstimulated cells were used as a negative control (M0). (A) The culture medium was collected, and nitrite were determined by the colorimetric Griess test. (B) The culture medium was collected to evaluate TNF-α production by ELISA. The results are presented as the means ± SEM for triplicate wells per group [*$p \leq 0.05$ compared to the M0 group; + $p \leq 0.05$ compared to the untreated group]. ND = not detectable.

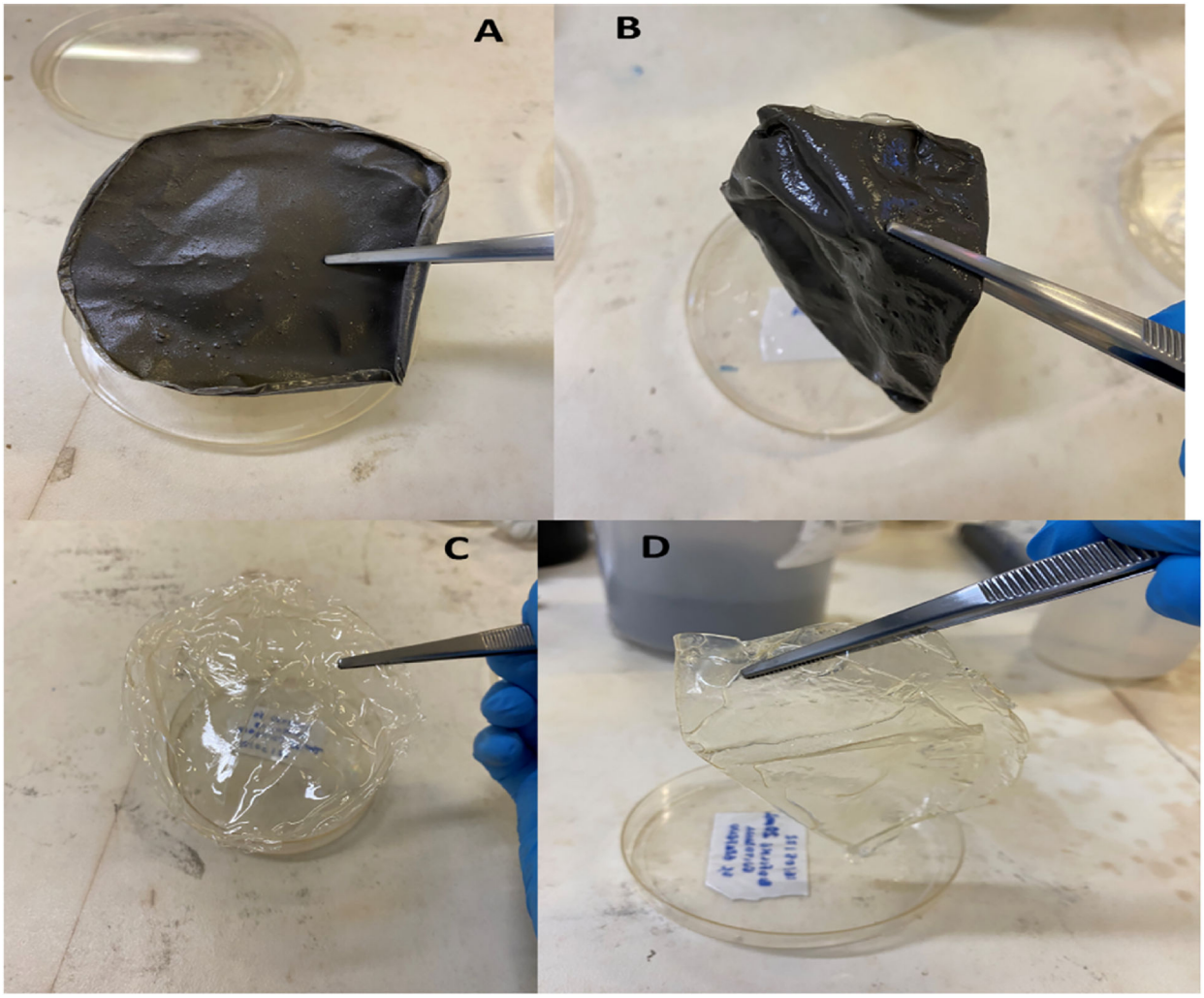

Fig. 10.

Swelling assay showing the ability of the film to absorb water. A shows the dried chitosan-GQDs film and B shows the chitosan-GQD film at the end of the assay. C shows the dried chitosan film and D shows the chitosan film at the end of the assay.

Table 1

Mass of water absorbed in the prepared films.

Film	Initial Mass (g)	Final Mass
Chitosan film	0.3830 ± 0.02	0.7033 ± 0.19
Chitosan-GQD film	1.782 ± 0.08	2.619 ± 0.89
Mass of water absorbed	1.399 ± 0.56	1.9157 ± 0.76